(Received 11 February 2026, Accepted 22 April 2026, Scheduled 30 April 2026)

Fixed-Condition Spoof Plasmonic Parametric Amplifier for Multi-Carrier Signals

Wen Yi Cui, Yue Cen, and Jingjing Zhang*

State Key Laboratory of Millimeter Waves, Southeast University, Nanjing 211189, China

ABSTRACT: To achieve synchronous and uniform amplification of dense multi-carrier signals, this paper proposes a multi-frequency nondegenerate parametric amplifier (PA) based on a nonlinear spoof surface plasmon polariton (SSPP) waveguide. By engineering the dispersion characteristics of a varactor-diode-loaded waveguide, we realize an SSPP platform that exhibits minimized phase mismatch for three distinct signal-idler pairs under a constant pump frequency (13.348 GHz) and a fixed bias voltage. Experimental results show that the amplifier delivers highly uniform gains exceeding 20 dB for three closely spaced carriers at 6.363, 6.489, and 6.549 GHz, effectively emulating a three-frequency-shift keying (3FSK) signal. This work demonstrates a fixed-condition amplification scheme that requires no dynamic tuning, offering a promising solution for amplifying densely spaced carriers in integrated communication systems.

1. INTRODUCTION

As new-generation wireless communication systems evolve toward high spectral efficiency, the adoption of dense multi-carrier modulation (e.g., multiple frequency-shift keying) has become a significant technological approach. However, in such systems, achieving synchronous, uniform, and low-distortion amplification when the multiple carrier frequencies are closely spaced poses a major challenge. The inherent nonlinearity of traditional amplifiers introduces severe intermodulation distortion, exacerbating the interference between carriers and degrading signal integrity [1, 2]. This challenge is even more prominent in highly integrated on-chip systems, often forcing the system to rely on complex multi-stage filtering or dynamic regulation circuits for compensation, significantly increasing the complexity, size, and power consumption [3]. Therefore, exploring a new platform from the perspective of fundamental electromagnetic interconnections and signal processing architectures that is compatible with high-density integration while possessing strong field localization and low nonlinear distortion characteristics is a key to overcoming the aforementioned challenges.

Spoof surface plasmon polaritons (SSPPs), an artificially engineered surface wave mode, provide a promising platform to address these technical challenges [4–9]. SSPPs support strong field confinement and low-loss propagation in the microwave frequencies by localizing electromagnetic energy within subwavelength or deep-subwavelength scales, akin to the optical surface plasmons [10–12], which at visible and near-infrared wavelengths have been widely utilized in sensing [13–17]. This characteristic not only enhances the nonlinear conversion efficiency and facilitates the device miniaturization [18, 19] but also suppresses the inter-channel electromagnetic interference effectively [20–22], illustrating considerable potential for highly integrated systems [23, 24], as well as for emerging SSPP-based biosensors [25] and antenna feeders [26, 27]. The dispersion of SSPPs is highly designable, enabling a variety of functionalities such as wavefront multiplexing [28], chromatic aberration correction [29], and broadband cloaking [30]. In particular, this designability allows precise phase matching to be achieved already at the design stage [18, 31–37]. For active tunable SSPP units, by adjusting the bias voltage, the dispersion can be tuned dynamically to satisfy varying phase-matching requirements across different operation scenarios. Compared with the conventional transmission lines, the SSPP waveguides offer enhanced spatial flexibility for integrating nonlinear active components such as varactor diodes. By altering the bias voltage, the dispersion characteristics of SSPPs can be flexibly tuned [38–41] to meet different phase-matching conditions across various application scenarios. In the practical communication systems, however, the SSPP signals still experience transmission loss and thus require on-chip amplification to preserve the signal integrity. The traditional semiconductor amplifiers introduce substantial nonlinear distortion and phase noise. This issue is particularly pronounced for SSPPs, which have a larger wavenumber compared to free-space waves at the same frequency, leading to intensified phase distortion [42].

Parametric amplification, as an amplification mechanism based on the nonlinear three-wave mixing process [43–46], offers some advantages, such as phase insensitivity, low thermal loss, and low nonlinear distortion [18]. Parametric amplification based on the SSPP platform leverages the strengths of SSPP, where strong field confinement and tunable dispersion enhance the nonlinear efficiency and provide unique design freedom for precise phase matching. This synergy offers a promising route to efficient amplification in integrated systems. However, a central limitation is the strict phase-matching requirement, which confines most current SSPP parametric am-

* Corresponding author: Jingjing Zhang (zhangjingjing@seu.edu.cn).

plifiers to single-frequency operation. This is inadequate for modern dense multi-carrier systems, which require simultaneous and uniform amplification at multiple frequencies. Thus, advancing beyond single-frequency designs to achieve multi-frequency or broadband phase matching in SSPP parametric amplifiers is critical for their adoption in next-generation high-spectral-efficiency wireless communications.

To address this challenge, we propose and experimentally validate a parametric amplifier based on a nonlinear SSPP waveguide in this study. The device achieves uniform multi-frequency amplification under fixed operating conditions — with a single varactor capacitance, a fixed pump frequency, and no dynamic bias tuning. By dispersing the SSPP unit integrated with a varactor diode, we realize approximate phase matching for three signal-idler pairs, thereby enabling simultaneous amplification of three adjacent carriers using only one pump wave. The compact amplifier exhibits highly uniform gains exceeding 20 dB at 6.363, 6.489, and 6.549 GHz, demonstrating its potential for high-spectral-efficiency communication systems with dense carrier allocations. Thus, this study provides a key device-level foundation for future on-chip and potentially low-distortion amplification of multi-carrier modulated signals such as 3FSK.

2. DESIGN AND EXPERIMENTAL RESULTS

The amplification mechanism employed in this work is based on parametric amplification, whose physical foundation is the nondegenerate three-wave mixing process. In this process, a high-power pump wave with frequency f_p and a low-power signal wave with frequency f_s interact in a nonlinear medium. According to energy conservation, this interaction generates an idler wave with a frequency of $f_i = f_p - f_s$. Assuming that the signal, idler, and pump waves propagate along the z direction, then the electric fields of signal, idler, and pump waves can be respectively expressed as:

$$E_s(z) = A_s(z)\,\mathrm{e}^{\mathrm{i}k_s z - \mathrm{i}\omega_s t}, \quad E_i(z) = A_i(z)\,\mathrm{e}^{\mathrm{i}k_i z - \mathrm{i}\omega_i t},$$
$$E_p(z) = A_p(z)\,\mathrm{e}^{\mathrm{i}k_p z - \mathrm{i}\omega_p t}$$

where A_s, A_i, A_p, ω_s, ω_i, ω_p, k_s, k_i, and k_p are respectively the electric field amplitudes, angular frequencies, and propagation constants of the signal, idler, and pump waves. The propagation constant k is divided into real part k', representing the propagation phase, and imaginary part k'', representing the transmission loss. That is to say, $k_s = k_s' + ik_s''$, $k_i = k_i' + ik_i''$ and $k_p = k_p' + ik_p''$. For the three-wave mixing process in the undepleted pump regime, $A_p(z)$ is a constant value and $\mathrm{d}A_p(z)/\mathrm{d}z \approx 0$, so $A_p(z)$ can be written as A_p. In this case, the amplitudes of signal and pump waves satisfy the following differential equation:

$$\frac{\mathrm{d}^2 A_s(z)}{\mathrm{d}z^2} + (\mathrm{i}\Delta k' + \Delta k_1'')\frac{\mathrm{d}A_s(z)}{\mathrm{d}z} - \frac{\omega_s^2\omega_i^2\left|\chi_{eff}^{(2)}A_p\right|^2}{k_s k_i^* c_0^4}A_s(z)\,e^{-2k_p'' z} = 0, \tag{1}$$

in which $\Delta k' = k_s' + k_i' - k_p'$ indicates the phase mismatch, $\Delta k_1'' = k_p'' + k_i'' - k_s''$, $\Delta k_2'' = k_p'' - k_i'' + k_s''$, c_0 is the light velocity, and $\chi_{eff}^{(2)}$ is the second-order effective nonlinear coefficient. Detailed derivation is shown in Supplementary Note 1, and the derived signal gain after propagating across a distance L is:

$$G = \left|\frac{E_s(L)}{E_s(0)}\right|^2 = \left|\frac{(\alpha/\beta)\left[K_\alpha(\beta)I_\alpha\left(\beta e^{-k_p''L}\right) - I_\alpha(\beta)K_\alpha\left(\beta e^{-k_p''L}\right)\right] + K_\alpha'(\beta)I_\alpha\left(\beta e^{-k_p''L}\right) - I_\alpha'(\beta)K_\alpha\left(\beta e^{-k_p''L}\right)}{I_\alpha(\beta)K_\alpha'(\beta) - I_\alpha'(\beta)K_\alpha(\beta)}\right|^2 e^{-\left(k_p''+k_i''+k_s''\right)L}. \tag{2}$$

It is clear that, in nonlinear parametric processes, the conversion efficiency is fundamentally governed by the phase-matching condition. The wavevector mismatch, $\Delta k'$, quantifies the deviation from ideal phase matching between the interacting waves (e.g., pump, signal, and idler). A smaller $\Delta k'$ directly leads to a higher nonlinear conversion efficiency because it enables constructive interference of the generated waves along the propagation distance. When $\Delta k'$ is minimized or is close to zero, the power flow coherently accumulates from the pump to the signal and idler waves over a longer effective interaction length, thereby achieving effective amplification of the signal wave. Conversely, a large $\Delta k'$ results in periodic power back-conversion and destructive interference, thereby severely limiting the net efficiency. Supplementary Note 1 shows the signal gain as a function of the nonlinear propagation distance L for different values of $\Delta k'$. Therefore, achieving a low $\Delta k'$ — often through careful dispersion engineering, is critical to maximizing the performance of parametric devices such as amplifiers and frequency converters.

Equation (2) also indicates that the signal gain is independent of the input signal power, which theoretically results in very low amplitude nonlinear distortion. Furthermore, the gain equation contains no term that depends on the initial phases of the pump, signal, and idler waves. Therefore, nondegenerate parametric amplification is intrinsically phase-insensitive, meaning that it does not introduce additional significant phase noise or phase distortion to the signal. Thus, low distortion is expected from the parametric process.

Figure 1(a) illustrates the functional schematic of the amplification system. A high-power continuous pump wave and an emulated three-frequency-shift keying (3FSK) signal (containing three carrier frequencies f_{c1}, f_{c2}, and f_{c3}) are jointly fed into the nonlinear SSPP waveguide, whose dispersion is meticulously engineered to satisfy the phase-matching condition for multiple signal-idler wave pairs under a fixed diode capacitance and pump frequency. Thus, amplification of this multi-frequency signal is achieved without adjusting the bias

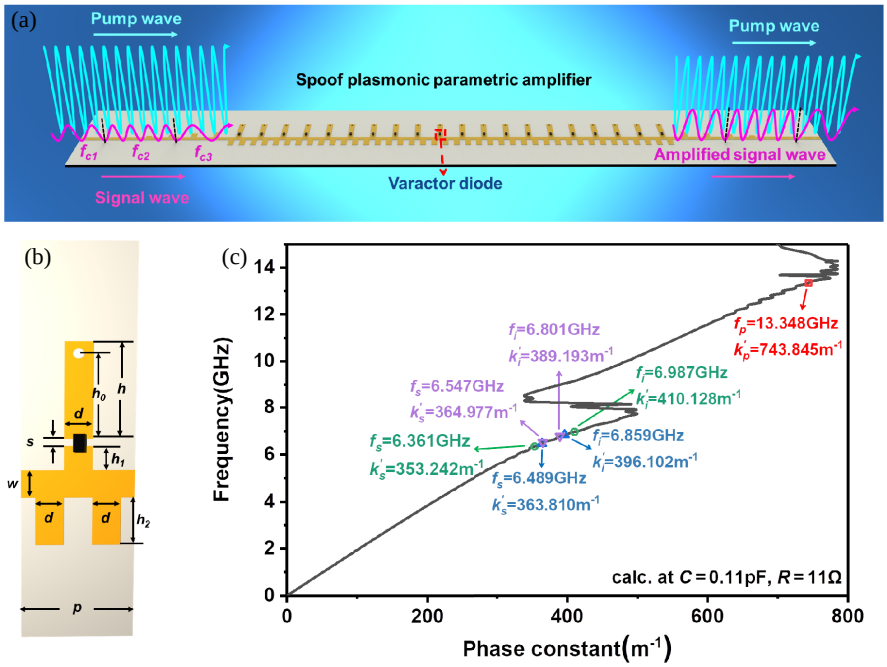

FIGURE 1. Design and operating principle of the multi-frequency nondegenerate parametric amplifier. (a) The schematic diagram of the SSPP parametric amplifier. (b) Geometry of the SSPP unit. (c) The calculated dispersion curve of the waveguide, indicating the three signal-idler wave pairs (sharing one pump wave) and the pump wave.

TABLE 1. Summary of frequencies, phase constants, and phase mismatches for the three nondegenerate signal-idler pairs (with $f_p = 13.348$ GHz).

Signal Frequency f_s (GHz)	Phase Constant k_s' (m^{-1})	Idler Frequency f_i (GHz)	Phase Constant k_i' (m^{-1})	Phase Mismatch $\Delta k'$ (m^{-1})
6.361	353.242	6.987	410.128	19.525
6.489	363.810	6.859	396.102	16.067
6.547	364.977	6.801	389.193	10.325

voltage or pump frequency. The designed SSPP waveguide employs a three-layer structure: the top layer is a periodically arranged corrugated metallic strip (thickness 0.018 mm); the middle layer is a Rogers RO 4350B dielectric substrate (thickness 0.508 mm, relative permittivity $\varepsilon_r = 3.66$, loss tangent $\tan\delta = 0.0037$); and the bottom layer is a complete metal ground plane (thickness 0.018 mm). Figure 1(b) shows the geometric dimensions of the waveguide unit, with a period $p = 4$ mm, tooth width $d = 1$ mm, center conductor width $w = 1.15$ mm, upper tooth heights $h = 4$ mm and $h_1 = 1$ mm, gap $s = 0.3$ mm, lower tooth height $h_2 = 2$ mm, and a grounding via with a radius of 0.2 mm and a center height of $h_0 = 3.5$ mm. The above geometric dimensions were determined through a systematic parameter sweep, and the detailed design methodology is presented in Supplementary Note 2.

The lossy dispersion curve in Figure 1(c) is extracted from simulated S-parameters of 44- and 45-unit SSPP waveguides using the method of [47, 48], which accounts for the varactor's resistance and eliminates transition effects. The propagation constant k is obtained from the eigenvalues of the transmission-matrix product, as detailed in the references. The frequencies and phase constants of the three experimentally observed signal-idler pairs with the highest gains are labeled in the figure and summarized in Table 1. The frequencies of the signal-idler pairs (f_s/f_i) are 6.361/6.987 GHz, 6.489/6.859 GHz, and 6.547/6.801 GHz, with corresponding phase mismatches of $\Delta k' = 19.525\,m^{-1}$, $16.067\,m^{-1}$, and $10.325\,m^{-1}$, respectively. Relative to the pump wave's phase constant $k_p' = 743.845\,m^{-1}$, these mismatches account for only 2.625%, 2.160%, and 1.388%, thereby satisfying the phase-matching conditions ($f_p = f_s + f_i$ and $k_p' = k_s' + k_i'$).

Based on the designed dispersion characteristics, we fabricated a nonlinear SSPP waveguide sample comprising $n = 45$ unit cells, as illustrated in Figure 2(a), and performed measurements to validate its performance. Figures 2(b) and (c) show the simulated and measured S-parameters of the SSPP-based parametric amplifier. In these plots, the solid vertical lines indicate the pump frequency f_p, whereas the dashed lines denote $f_p/2$ and the lower and upper bounds of the signal band under test. By fitting the simulated S_{21} curve to the measured one, with the varactor datasheet as a reference, we find that the simulated S_{21} curve at $C = 0.11$ pF and $R = 11\,\Omega$ agrees well with the measured S_{21} curve when a DC bias of 1.8 V is applied to

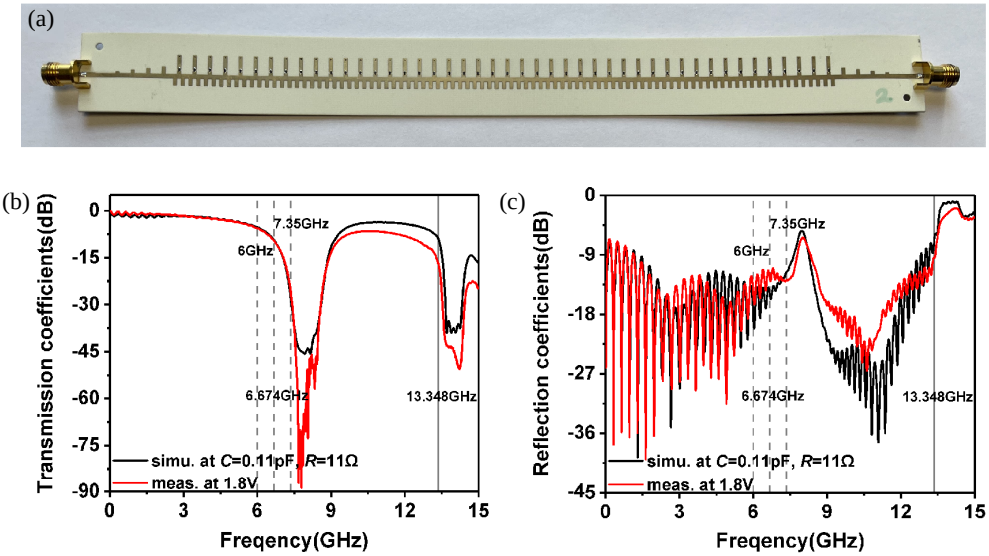

FIGURE 2. Nonlinear SSPP waveguide and its S-parameters. (a) Photograph of the 45-unit SSPP waveguide. (b) Simulated and measured S_{21} curves of the SSPP waveguide. (c) Simulated and measured S_{11} curves of the SSPP waveguide.

the varactor. Thus, the varactor resistance is 11 Ω, and a bias of 1.8 V corresponds to a capacitance of 0.11 pF.

As the SSPP wave approaches its cutoff frequency, the field confinement strengthens, thereby enhancing the nonlinear response. Consequently, despite the relatively low transmission coefficient of the pump wave, the SSPP parametric amplifier still yields substantial parametric gain. At the three phase-matched signal frequencies (6.361 GHz, 6.489 GHz, and 6.547 GHz), the measured transmission coefficients are −7.36 dB, −7.99 dB, and −8.46 dB, respectively, whereas the measured reflection coefficients are −11.77 dB, −14.19 dB, and −12.93 dB, respectively. These results indicate a moderate intrinsic insertion loss for the signal waves along the SSPP waveguide, ensuring that linear transmission characteristics do not significantly compromise the achievable parametric gain.

The experimental setup used to measure the multi-frequency nondegenerate parametric gain is illustrated in Figure 3. The signal and pump waves were supplied by signal generators 1 (Agilent E8257D) and 2 (Keysight E8257D PSG), respectively. As achieving nondegenerate parametric amplification requires a relatively high-power pump, the input pump power p_p is boosted to approximately 27.05 dBm using a power amplifier. The high-power pump and signal waves to be amplified were coupled using a 16 dB directional coupler (Midwest Microwave CPL-5231-16-001-79) and then fed into the SSPP parametric amplifier. A DC bias voltage of 1.8 V was applied to the varactor diodes in the waveguide via a bias tee, which biases all 45 varactor diodes, whereas DC blocks were used to protect the instruments by preventing DC signals from passing through. The losses introduced by the bias tee and DC block were included in the total system loss and subtracted when calculating the signal gain. Finally, the amplified output signal was received and analyzed using a signal analyzer (Keysight N9040B).

Figure 4 shows the measured signal gain (left axis) versus signal frequency under the fixed pump condition designed in this work ($f_p = 13.348$ GHz, $p_p = 27.05$ dBm). Overlaid on the same figure (right axis) is the measured S_{21} curve of the SSPP waveguide under the pump-off condition, indicating the passive loss. In the frequency band of 6–7.35 GHz, the gain spectrum exhibits multiple distinct peaks. Among these peaks, the three nondegenerate signal-idler pairs, namely, 6.361/6.987 GHz, 6.489/6.859 GHz, and 6.547/6.801 GHz, show the most prominent gains, all exceeding 19 dB. The red reference line at 20.815 dB marks the smallest gain among these three nondegenerate signal peaks (at 6.489 GHz), which is used as the baseline for selecting the three carrier frequencies for the emulated 3FSK signal. The gains at 6.859 GHz and 6.987 GHz lie slightly below this reference line owing to their proximity to the waveguide cutoff, where a higher transmission loss is incurred and subsequently subtracted during calibration. The highest peak of 31.14 dB occurs at the degenerate point ($f_s = f_i = f_p/2 = 6.674$ GHz). The degenerate gain is phase-sensitive because the signal and idler share the same frequency and thus interfere [35]. This reported value represents the maximum gain achieved by adjusting the pump phase to enforce constructive interference between the signal and generated idler waves. Additional gain measurements under different pump powers and with the pump frequency shifted away from the designed phase-matching point (i.e., $f_p = 13.148$ GHz and 13.548 GHz) are discussed in Supplementary Note 3, further validating the importance of phase matching.

As shown in Figure 4, the amplifier can be used to amplify the 3FSK signals. To avoid interference from the idler waves that are difficult to filter out, we selected three nondegenerate gain peaks on the same side (left) of the degenerate peak as the carrier frequencies. This ensures that the corresponding idlers are generated on the opposite side, facilitating filtering in practical systems. Furthermore, to prevent amplitude distortion, the gain at each carrier must be equalized. Using the lowest of the three nondegenerate gains (about 20.815 dB at 6.489 GHz) as a reference, we chose three frequencies with gains around this

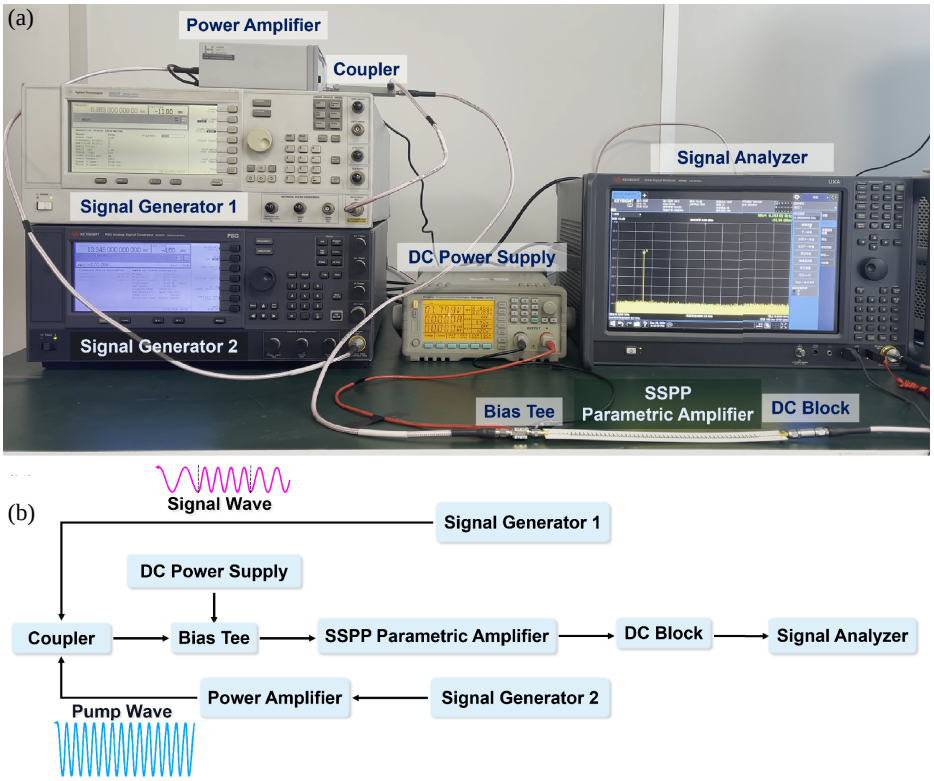

FIGURE 3. Experimental setup employed to measure multi-frequency nondegenerate parametric amplification. (a) Photograph of the setup; (b) Block diagram of the experimental system.

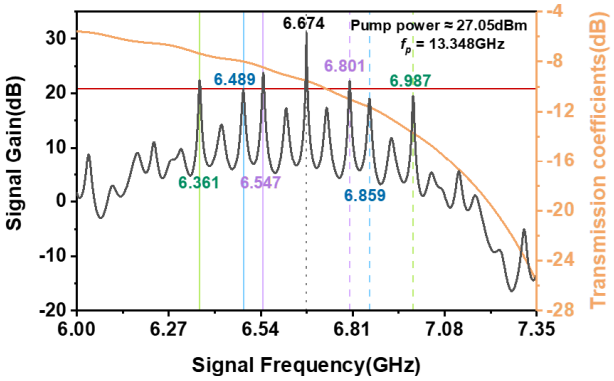

FIGURE 4. The measured signal gain versus the signal frequency under a pump power of 27.05 dBm, with the pump frequency at the designed value ($f_p = 13.348$ GHz). The overlaid transmission coefficient curve (right axis) is measured under the pump-off condition, showing the passive transmission characteristic of the SSPP waveguide.

value (6.363 GHz, 6.489 GHz, and 6.549 GHz) as the 3FSK carriers. This demonstrates that the proposed SSPP parametric amplifier can achieve uniform amplification of a dense 3FSK signal under fixed bias and fixed pump conditions, eliminating the need for dynamic control.

To verify the actual amplification capability of the SSPP parametric amplifier for multi-carrier modulated signals, we used the frequency-sweep function of a signal generator to sequentially output continuous waves at three fixed carrier frequencies ($f_{c1} = 6.363$ GHz, $f_{c2} = 6.489$ GHz, $f_{c3} = 6.549$ GHz). This emulates a 3FSK-like signal that replicates the frequency-hopping behavior of a true 3FSK waveform.

The resulting output spectrum after passing the SSPP waveguide appears in Figure 5(b). Compared with Figure 5(a), this trace directly captures the transmission loss introduced by the waveguide. Owing to the SSPP dispersion, the attenuation varies slightly across the three carriers, leading to unequal output power levels. Firstly, to establish a reference baseline, the bias tee, SSPP waveguide, and DC block in the setup of Figure 3 were replaced by a through component while the pump remained off. The measured power spectrum of the emulated 3FSK signal in this through configuration is shown in Figure 5(a), with an average power of approximately −28.93 dBm. Next, the original setup (bias tee, SSPP waveguide, and DC block) was restored, still without injecting the pump. The output spectrum measured after the SSPP waveguide is shown in Figure 5(b). Compared with Figure 5(a), this spectrum directly reflects the transmission loss introduced by the SSPP waveguide. Owing to the dispersion characteristics of the SSPP, the attenuation varies slightly across the three carrier frequencies, resulting in unequal output power levels. Finally, keeping the above experimental setup unchanged, a pump wave at 13.348 GHz and an input power of approximately 27.05 dBm were applied. The output spectrum measured under this condition is presented in Figure 5(c). As shown, the signal power at all three carriers is increased significantly and uniformly to approximately −7.75 dBm, thereby compensating for the power imbalance caused by the waveguide transmission loss. Compared with the through power shown in Figure 5(a), the non-

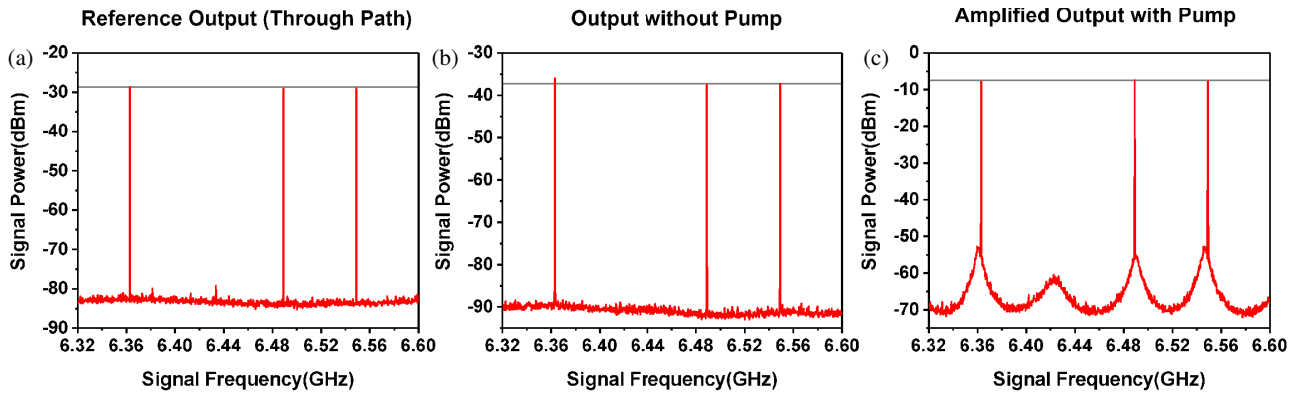

FIGURE 5. Output power spectra of the emulated 3FSK signal under three test conditions. (a) Reference output spectrum with a through component replacing the SSPP waveguide. (b) Output spectrum after transmission through the SSPP waveguide without a pump-wave input. (c) Output spectrum after amplification by the SSPP waveguide with a pump-wave input.

TABLE 2. Comparison of key parameters among representative parametric amplifiers.

Parameter	Gain	Working frequency band (fixed condition)	Dynamic tuning required	Operating temperature	Compatibility with planar integration
Superconducting JPA [49]	20 dB over 200 MHz	0.2 GHz at 20 dB gain, 0.7 GHz at 15 dB gain	Yes (magnetic flux and pump frequency)	About 20 mK	Low (mK-level cryogenic environment required)
Nondegenerate SSPP PA [18]	Up to 9.14 dB	Single frequency point	Yes (bias voltage)	Room temperature	High
Degenerate SSPP PA [35]	−33 dB to 22 dB (phase-tunable)	Single frequency point	Yes (phase difference)	Room temperature	High
This work	Over 20 dB	Three non-continuous frequency points	No	Room temperature	High

degenerate parametric amplification delivers a gain of about 21.18 dB at each target carrier.

Dynamic demonstration videos of the test configurations are provided as supplementary material. The results confirm that the proposed SSPP parametric amplifier achieves high-gain and low-distortion amplification of dense multi-carrier signals under fixed operating conditions, underscoring its potential for on-chip signal processing in high-spectral-efficiency communication systems.

As summarized in Table 2, previous SSPP-based parametric amplifiers [18, 35] operate only at a single frequency under any fixed condition. The nondegenerate SSPP amplifier in [18] achieves a peak gain of 9.14 dB at a single frequency (3.69 GHz) under optimal bias. Although its matching frequency can be reconfigured over a range of 0.62 GHz by adjusting the bias voltage, the gain drops substantially when it moves away from the optimal point, and only one frequency can be amplified at a time. The degenerate SSPP amplifier in [35] operates at a fixed frequency (4.46 GHz) and offers phase-tunable gain from −33 dB to 22 dB by adjusting the relative phase between the input pump and signal waves. Note that degenerate parametric amplification is phase-sensitive, which may introduce phase distortion.

The cryogenic Josephson parametric amplifier [49] provides a continuous bandwidth (e.g., 0.2 GHz for 20 dB gain, 0.7 GHz for 15 dB gain) under a fixed operating condition, and its center frequency can be tuned over 1.4 GHz by changing the magnetic flux. However, it requires a very low temperature (about 20 mK) and has an extremely low input saturation power (about −110 dBm), making it impractical for room-temperature communication signals. In sharp contrast, our nondegenerate SSPP parametric amplifier simultaneously satisfies the phase-matching condition for three distinct non-continuous frequencies (6.363, 6.489, and 6.549 GHz) under a fixed pump frequency (13.348 GHz) and fixed bias voltage (1.8 V), delivering over 20 dB uniform gain at room temperature without any dynamic tuning, and features a measured input saturation power of approximately −28.5 dBm (see Supplementary Note 1). To the best of our knowledge, this is the first demonstration of a parametric amplifier capable of concurrent high-gain amplification at multiple carriers in a fixed-condition setting.

3. CONCLUSION

This study presents a multi-frequency nondegenerate parametric amplifier based on a nonlinear SSPP waveguide. By strategically designing the waveguide dispersion, we experimentally realized the uniform amplification of three closely spaced carriers under fixed operating conditions, a constant pump frequency and a fixed bias voltage. The amplifier achieved over 20 dB of gain for each carrier in a 3FSK-emulated signal, ef-

fectively compensating for the inherent transmission loss variations. This fixed-condition configuration eliminates the need for complex and dynamic controls, thereby significantly reducing system complexity. These results may offer practical and efficient solutions for on-chip reconfigurable front-ends in future high-spectral-efficiency communication systems, in which theoretically low distortion and multichannel signal processing are paramount. The proposed dispersion-engineering strategy has the potential to be extended towards higher-order (beyond 3FSK) multi-carrier systems by further broadening the signal phase-matching bandwidth.

ACKNOWLEDGEMENT

This work was supported by the National Natural Science Foundation of China (grant numbers 62271139 and U25A20411), the National Key Research and Development Program of China (grant number 2022YFA1404903), and the Postgraduate Research & Practice Innovation Program of Jiangsu Province (grant number 3304002304D).

REFERENCES

[1] Cripps, S., *Advanced Techniques in RF Power Amplifier Design*, Artech House, Norwood, Massachusetts, 2002.

[2] Meindl, J. D., "Beyond Moore's law: The interconnect era," *Computing in Science & Engineering*, Vol. 5, No. 1, 20–24, Jan. 2003.

[3] Dowla, F., *Handbook of RF and Wireless Technologies*, Newnes, Amsterdam, 2004.

[4] Cui, T. J., "Microwave metamaterials — From passive to digital and programmable controls of electromagnetic waves," *Journal of Optics*, Vol. 19, No. 8, 084004, 2017.

[5] Joy, S. R., M. Erementchouk, H. Yu, and P. Mazumder, "Spoof plasmon interconnects — Communications beyond RC limit," *IEEE Transactions on Communications*, Vol. 67, No. 1, 599–610, Jan. 2019.

[6] Zhang, J., H.-C. Zhang, X.-X. Gao, L.-P. Zhang, L.-Y. Niu, P.-H. He, and T.-J. Cui, "Integrated spoof plasmonic circuits," *Science Bulletin*, Vol. 64, No. 12, 843–855, Jun. 2019.

[7] Zhang, H. C., P. H. He, W. X. Tang, Y. Luo, and T. J. Cui, "Planar spoof SPP transmission lines: Applications in microwave circuits," *IEEE Microwave Magazine*, Vol. 20, No. 11, 73–91, Nov. 2019.

[8] Tang, W. X., H. C. Zhang, H. F. Ma, W. X. Jiang, and T. J. Cui, "Concept, theory, design, and applications of spoof surface plasmon polaritons at microwave frequencies," *Advanced Optical Materials*, Vol. 7, No. 1, 1800421, Jan. 2019.

[9] Garcia-Vidal, F. J., A. I. Fernández-Domínguez, L. Martin-Moreno, H. C. Zhang, W. Tang, R. Peng, and T. J. Cui, "Spoof surface plasmon photonics," *Reviews of Modern Physics*, Vol. 94, No. 2, 025004, May 2022.

[10] Pendry, J. B., L. Martín-Moreno, and F. J. Garcia-Vidal, "Mimicking surface plasmons with structured surfaces," *Science*, Vol. 305, No. 5685, 847–848, 2004.

[11] Shen, X., T. J. Cui, D. Martin-Cano, and F. J. Garcia-Vidal, "Conformal surface plasmons propagating on ultrathin and flexible films," *Proceedings of the National Academy of Sciences*, Vol. 110, No. 1, 40–45, 2013.

[12] Zhang, H. C., Q. Zhang, J. F. Liu, W. Tang, Y. Fan, and T. J. Cui, "Smaller-loss planar SPP transmission line than conventional microstrip in microwave frequencies," *Scientific Reports*, Vol. 6, No. 1, 23396, Mar. 2016.

[13] Chou Chau, Y.-F., "Advances in Fano resonance-based metal-insulator-metal plasmonic sensors: Mechanisms, applications, and future perspectives," *Optics & Laser Technology*, Vol. 194, 114487, Feb. 2026.

[14] Chou Chau, Y.-F., Y.-J. Lin, and D. P. Tsai, "Enhanced surface plasmon resonance based on the silver nanoshells connected by the nanobars," *Optics Express*, Vol. 18, No. 4, 3510–3518, Feb. 2010.

[15] Chou Chau, Y.-F., "Multiple-mode bowtie cavities for refractive index and glucose sensors working in visible and near-infrared wavelength ranges," *Plasmonics*, Vol. 16, No. 5, 1633–1644, 2021.

[16] Chou Chau, Y.-F. C., S.-H. Chen, A. H. Mahadi, R. Thotagamuge, C. M. Lim, and M. R. R. Kooh, "Plasmonic-heterojunction nanostructures: Mechanistic design for photocatalysis, energy conversion, and advanced biosensing," *Sustainable Materials and Technologies*, Vol. 47, e01833, Apr. 2026.

[17] Chou Chau, Y.-F., H.-H. Yeh, and D. P. Tsai, "Surface plasmon effects excitation from three-pair arrays of silver-shell nanocylinders," *Physics of Plasmas*, Vol. 16, No. 2, 022303, Feb. 2009.

[18] Gao, X., J. Zhang, Y. Luo, Q. Ma, G. D. Bai, H. C. Zhang, and T. J. Cui, "Reconfigurable parametric amplifications of spoof surface plasmons," *Advanced Science*, Vol. 8, No. 17, 2100795, Sep. 2021.

[19] Cui, W. Y., X. Gao, J. Zhang, Y. Luo, and T. J. Cui, "Power-modulated reconfigurable nonlinear plasmonic devices without DC power supply and feed circuit," *npj Nanophotonics*, Vol. 1, No. 1, 11, Jun. 2024.

[20] Zhang, H. C., T. J. Cui, Q. Zhang, Y. Fan, and X. Fu, "Breaking the challenge of signal integrity using time-domain spoof surface plasmon polaritons," *ACS Photonics*, Vol. 2, No. 9, 1333–1340, 2015.

[21] Gao, X., H. C. Zhang, P. H. He, Z. X. Wang, J. Lu, R. T. Yan, and T. J. Cui, "Crosstalk suppression based on mode mismatch between spoof SPP transmission line and microstrip," *IEEE Transactions on Components, Packaging and Manufacturing Technology*, Vol. 9, No. 11, 2267–2275, Nov. 2019.

[22] Zhang, H. C., L. P. Zhang, P. H. He, J. Xu, C. Qian, F. J. Garcia-Vidal, and T. J. Cui, "A plasmonic route for the integrated wireless communication of subdiffraction-limited signals," *Light: Science & Applications*, Vol. 9, No. 1, 113, Jul. 2020.

[23] Zhang, H. C., W. X. Tang, J. Xu, S. Liu, J. F. Liu, and T. J. Cui, "Reduction of shielding-box volume using SPP-like transmission lines," *IEEE Transactions on Components, Packaging and Manufacturing Technology*, Vol. 7, No. 9, 1486–1492, Sep. 2017.

[24] Lu, J., H. C. Zhang, P. H. He, L. P. Zhang, and T. J. Cui, "Design of miniaturized antenna using corrugated microstrip," *IEEE Transactions on Antennas and Propagation*, Vol. 68, No. 3, 1918–1924, Mar. 2020.

[25] Imamvali, S., K. Prakash, S. Bansal, S. Tupakula, A. K. Suresh, A. J. A. Al-Gburi, M. R. I. Faruque, and K. S. Al-Mugren, "Label-free biosensing of persistent organic pollutants in sewage water using spoof surface plasmon polaritons," *Sensors and Actuators A: Physical*, Vol. 388, 116504, Jul. 2025.

[26] Chaparala, R., S. Imamvali, S. Tupakula, M. Aljaidi, S. Bansal, K. Prakash, and A. F. Alkoradees, "Optimizing dielectric rod antenna performance with spoof surface plasmon polariton-based feeding method," *Sensors*, Vol. 24, No. 23, 7543, Nov. 2024.

[27] Chaparala, R., S. Imamvali, S. Tupakula, K. Prakash, S. Bansal, M. M. Ismail, and A. J. A. Al-Gburi, "Spoof surface plasmon

polaritons-based feeder for a dielectric rod antenna at microwave frequencies," *Progress In Electromagnetics Research M*, Vol. 129, 23–32, 2024.

[28] Guan, C., T. Cai, L. Zhu, J. Han, C. Ding, S. N. Burokur, Q. Wu, and X. Ding, "Guided and space waves multiplexed metasurface for advanced electromagnetic functionalities in microwave region," *Advanced Materials*, Vol. 37, No. 7, 2417724, Feb. 2025.

[29] Cai, T., S. Tang, B. Zheng, G. Wang, W. Ji, C. Qian, Z. Wang, E. Li, and H. Chen, "Ultrawideband chromatic aberration-free meta-mirrors," *Advanced Photonics*, Vol. 3, No. 1, 016001, Dec. 2020.

[30] Cai, T., B. Zheng, J. Lou, L. Shen, Y. Yang, S. Tang, E. Li, C. Qian, and H. Chen, "Experimental realization of a superdispersion-enabled ultrabroadband terahertz cloak," *Advanced Materials*, Vol. 34, No. 38, 2205053, Sep. 2022.

[31] Liu, L., L. Wu, J. Zhang, Z. Li, B. Zhang, and Y. Luo, "Backward phase matching for second harmonic generation in negative-index conformal surface plasmonic metamaterials," *Advanced Science*, Vol. 5, No. 11, 1800661, Nov. 2018.

[32] Gao, X., J. Zhang, H. C. Zhang, L. Liu, Q. Ma, P. Xu, and T. J. Cui, "Dynamic controls of second-harmonic generations in both forward and backward modes using reconfigurable plasmonic metawaveguide," *Advanced Optical Materials*, Vol. 8, No. 8, 1902058, Apr. 2020.

[33] Liu, X., Y. Lei, X. Zheng, Y. Ren, X. Gao, J. Zhang, and T. J. Cui, "Reconfigurable spoof plasmonic coupler for dynamic switching between forward and backward propagations," *Advanced Materials Technologies*, Vol. 7, No. 8, 2200129, Aug. 2022.

[34] Gao, X., J. Zhang, Q. Ma, W. Y. Cui, Y. Ren, Y. Luo, and T. J. Cui, "Nonmagnetic spoof plasmonic isolator based on parametric amplification," *Laser & Photonics Reviews*, Vol. 16, No. 4, 2100578, Apr. 2022.

[35] Cui, W. Y., J. Zhang, Y. Luo, X. Gao, and T. J. Cui, "Dynamic switching from coherent perfect absorption to parametric amplification in a nonlinear spoof plasmonic waveguide," *Nature Communications*, Vol. 15, No. 1, 2824, Apr. 2024.

[36] Cui, W. Y. and J. Zhang, "Nonlinear coherent perfect absorption based on second harmonic generation in a spoof plasmonic waveguide," in *2024 Cross Strait Radio Science and Wireless Technology Conference (CSRSWTC)*, 1–3, Macao, China, Nov. 2024.

[37] Cui, W., X. Gao, and J. Zhang, "Bidirectional-pump-controlled reconfigurable nonlinear spoof plasmonic waveguide," *Frontiers of Information Technology & Electronic Engineering*, Vol. 26, No. 11, 2382–2392, Nov. 2025.

[38] Zhang, H. C., T. J. Cui, J. Xu, W. Tang, and J. F. Liu, "Real-time controls of designer surface plasmon polaritons using programmable plasmonic metamaterial," *Advanced Materials Technologies*, Vol. 2, No. 1, 1600202, Jan. 2017.

[39] Zhang, L., H. Zhang, M. Tang, P. He, L. Niu, L. Liu, J. Lu, W. Tang, J. Mao, and T. Cui, "Integrated multi-scheme digital modulations of spoof surface plasmon polaritons," *Science China Information Sciences*, Vol. 63, No. 10, 202302, 2020.

[40] Zhang, H. C., T. J. Cui, Y. Luo, J. Zhang, J. Xu, P. H. He, and L. P. Zhang, "Active digital spoof plasmonics," *National Science Review*, Vol. 7, No. 2, 261–269, Feb. 2020.

[41] Gao, X., Z. Gu, Q. Ma, W. Y. Cui, T. J. Cui, and C. H. Chan, "Reprogrammable spoof plasmonic modulator," *Advanced Functional Materials*, Vol. 33, No. 18, 2212328, May 2023.

[42] Zhang, H. C., S. Liu, X. Shen, L. H. Chen, L. Li, and T. J. Cui, "Broadband amplification of spoof surface plasmon polaritons at microwave frequencies," *Laser & Photonics Reviews*, Vol. 9, No. 1, 83–90, Jan. 2015.

[43] Armstrong, J. A., N. Bloembergen, J. Ducuing, and P. S. Pershan, "Interactions between light waves in a nonlinear dielectric," *Physical Review*, Vol. 127, No. 6, 1918, Sep. 1962.

[44] Boyd, G. D. and D. A. Kleinman, "Parametric interaction of focused gaussian light beams," *Journal of Applied Physics*, Vol. 39, No. 8, 3597–3639, Jul. 1968.

[45] Stolen, R. and J. Bjorkholm, "Parametric amplification and frequency conversion in optical fibers," *IEEE Journal of Quantum Electronics*, Vol. 18, No. 7, 1062–1072, Jul. 1982.

[46] Boyd, R. W., *Nonlinear Optics*, 4th ed., Academic Press, 2020.

[47] Zhang, X., H. C. Zhang, W. X. Tang, J. F. Liu, Z. Fang, J. W. Wu, and T. J. Cui, "Loss analysis and engineering of spoof surface plasmons based on circuit topology," *IEEE Antennas and Wireless Propagation Letters*, Vol. 16, 3204–3207, 2017.

[48] Zhang, L. P., H. C. Zhang, Z. Gao, and T. J. Cui, "Measurement method of dispersion curves for spoof surface plasmon polaritons," *IEEE Transactions on Antennas and Propagation*, Vol. 67, No. 7, 4920–4923, Jul. 2019.

[49] Qing, B., L. B. Nguyen, X. Liu, H. Ren, W. P. Livingston, N. Goss, A. Hajr, T. Chistolini, Z. Pedramrazi, D. I. Santiago, J. Luo, and I. Siddiqi, "Broadband coplanar-waveguide-based impedance-transformed josephson parametric amplifier," *Physical Review Research*, Vol. 6, No. 1, L012035, Feb. 2024.